Journal of the Mechanics and Physics of Solids 133 (2019) 103705

Contents lists available at ScienceDirect

Journal of the Mechanics and Physics of Solids

journal homepage: www.elsevier.com/locate/jmps

Electrostatic switching of nuclear basket conformations provides a potential mechanism for nuclear mechanotransduction

Shaobao Liu[a,b,c], Haiqian Yang[c,d], Tian Jian Lu[a,d], Guy M. Genin[b,c,e], Feng Xu[b,c,*]

[a] State Key Laboratory of Mechanics and Control of Mechanical Structures, Nanjing University of Aeronautics and Astronautics, Nanjing 210016, PR China
[b] MOE Key Laboratory of Biomedical Information Engineering, School of Life Science and Technology, Xi'an Jiaotong University, Xi'an 710049, PR China
[c] Bioinspired Engineering and Biomechanics Center (BEBC), Xi'an Jiaotong University, Xi'an 710049, PR China
[d] State Key Laboratory for Strength and Vibration of Mechanical Structures, Xi'an Jiaotong University, Xi'an 710049, PR China
[e] National Science Foundation Science and Technology Center for Engineering Mechanobiology, Washington University, St. Louis, MO 63130, United States

ARTICLE INFO

Article history:
Received 14 January 2019
Revised 30 August 2019
Accepted 30 August 2019
Available online 30 August 2019

Keywords:
Nuclear pore complex
Mechanotransduction
Bi-stable switches
Debye screening

ABSTRACT

Cells can respond to mechanical forces by changing gene expression. Changes to transport through pores in the nuclear membrane have been implicated in these responses, but the mechanisms by which stress-dependent, selective nuclear transport occur have not been elucidated. We identified a potential mechanism for this via stretch-dependent switching behavior in nuclear pore complexes (NPCs). NPCs, composed of proximal and distal rings connected by a "basket" of filaments within the nucleus, form channels for the selective transport through the nuclear membrane. Our simulations showed that the relatively narrow NPC distal ring, long believed to responsible for channel gating and selectivity, cannot stretch to accommodate larger molecules. Instead, our results suggested that rapid phase transitions in nuclear basket filament conformations could serve to regulate large molecule transport. Nuclear basket conformations were bi-stable under certain conditions within the physiological range, enabling strong sensitivity to the mechanical state of the nuclear membrane, and suggesting a possible pathway for mechanosensitive nuclear gating.

1. Introduction

The ways that mechanical signals are felt and remembered by cells are largely unknown, but are critical to growth, development, and pathology (Dupont et al., 2011; Tschumperlin et al., 2004). Because gene expression and cell fate can be altered by mechanical force, efforts to identify ways that mechanical deformation can affect gene expression have been of intense focus (Cao et al., 2017; Engler et al., 2006; Makhija et al., 2016; Meng et al., 2018; Nathan et al., 2011; Poleshko et al., 2017; Swift et al., 2013b). Proteins in the LINC complex are known to transmit forces felt and exerted by cells to the nuclear envelope, and to rearrange molecules in the cytoplasm to open pathways for mechanosensing molecules to reach the nuclear envelope (Crisp et al., 2006). Nuclear pore complexes (NPCs) are known to be involved in selective transport of molecules

* Corresponding author.
E-mail address: fengxu@mail.xjtu.edu.cn (F. Xu).

https://doi.org/10.1016/j.jmps.2019.103705
0022-5096/

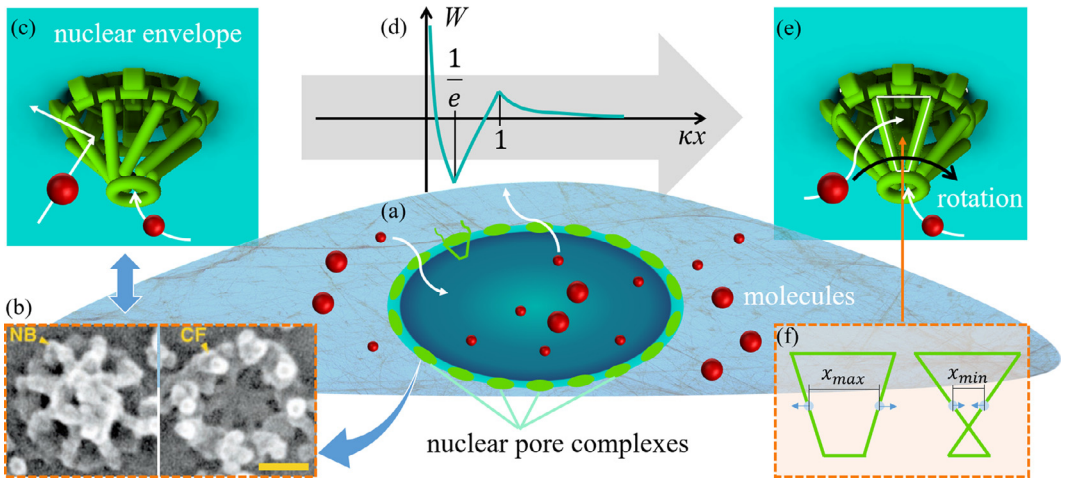

Fig. 1. Phase transitions in nuclear basket conformations provide a potential mechanism for nuclear mechanotransduction. (a) Nuclear pore complexes (NPCs) gate traffic between the nucleus and the cytoplasm. We explored whether these might contribute to nuclear mechanotransduction. (b) Scanning electron microscopy of a vertebrate (*Xenopus*) NPC viewed *en face* from the cytoplasm best reveals the cytoplasmic filaments (CF, right panel); a view from the nucleoplasm reveals the nuclear basket (NB, left panel) (reprinted with permission from Rout and Aitchison (2001)). (scale bar, 30 nm). (c) The initially twisted nuclear basket allowed only small molecules to pass through the NPC. (d) NPC conformations were a balance between elastic energy in the membrane and electrostatic interaction energy (W) NPC filaments, the latter governed by a dimensionless spacing $\boldsymbol{\kappa x}$, in which $\boldsymbol{\kappa}$ is the Debye screening parameter. (e) Our models suggested that sufficient nuclear envelope stretch can lead to new conformations of the NPC, some of which may enable transport of larger molecules through the NPCs. Bi-stable conformations might explain the stretch-dependent translocation through nuclear pores of signaling molecules, as reported recently by Elosegui-Artola et al. (2017). (f) These conformations were limited by steric constraints.

across the nuclear envelope (Gallardo et al., 2017; Ghavami et al., 2014; Mario et al., 2013) (Fig. 1a). Mutations in NPCs affect cell differentiation, function, and aging (Burns and Wente, 2014; Lord et al., 2015). Stressing of the nuclear envelope can trigger entry of the mechanosensing molecule YAP to the nucleus via transport through NPCs (Elosegui-Artola et al., 2017). However, it is not known how relatively small mechanical changes can enable switching of these NPCs.

We therefore asked whether the gating of NPCs might enhance sensitivity to mechanical stretch sufficiently to enable stretch-dependent gating. The 30–70 nm diameter channel of NPCs is the core of an octagonal protein structure consisting of cytoplasmic and nucleoplasmic rings inserting into the nuclear membrane, a “nuclear basket” of filaments extending into the nucleoplasm, and a distal ring connecting these filaments at the innermost extremity of the NPC (Ghavami et al., 2014; Mario et al., 2013) (Fig. 1b, c & e). Effective and selective transport occurs through the NPC at rates on the order of 1000 translocations per second, and includes transport of mRNA and molecules over 40 kDa (Garcia et al., 2016; Jamali et al., 2011). The nuclear basket ultrastructure functions as a docking site for messenger ribonucleoprotein and reduces chromatin crowding around the central transport channel. The nuclear basket is generally depicted as a relatively rigid structure of eight protein filaments that protrude into the nucleoplasm and converge in the distal ring (Fig. 1). This distal ring is believed to serve as the primary gatekeeper for mRNA, silencing factors, and cell cycle regulators (Gallardo et al., 2017). The relationship between the morphology and function of NPCs has largely been studied through an axisymmetric model of the nuclear basket (Ma and Lippincott-Schwartz, 2010; Moussavibaygi et al., 2011; Rout and Aitchison, 2001; Solmaz et al., 2011). Fluctuations of the iris-like (rotationally symmetric) distal ring are believed to control transport of large molecules (Arlucea et al., 1998; Kramer et al., 2008; Sakiyama et al., 2017) in a way that is dependent on calcium ions (Panté and Aebi, 1996; Stoffler et al., 1999a). Torsional (rotationally symmetric) conformations of the nuclear basket have been identified as affecting function in models and experiment (Akey and Radermacher, 1993; Garcia et al., 2016; Rout and Aitchison, 2001; Yang et al., 1998).

However, the transport of larger molecules cannot be explained by the distal ring model alone, and the mechanisms of stress-dependent entry of YAP through NPCs remains a mystery. Cargo-receptor-gold complexes with diameters as large as 39 nm – 33% larger than the largest distal ring observed – have been observed passing through NPCs (Panté and Kann, 2002). The static view of the nuclear basket might be an oversimplification in light of observations of multiple filament conformations under identical electromechanical conditions (Arlucea et al., 1998), and of a range of observed NPC deformation modes (Wolf and Mofrad, 2008).

Forces on the nuclear pore basket arise from chemical bonding, mechanical forces arising from Brownian motion, and electrostatic forces. We focused on relatively short-range electrostatic forces arising from charge condensation because scaling arguments described in the methods section indicated that these would be significant, and because other forces could be ruled out for the following reasons. First, experimental observations reveal that the nuclear pore basket represents a loose structure whose shape could transform via mechanisms consistent with a space truss (Panté and Aebi, 1996; Stoffler et al., 1999a), ruling out an important role for relatively strong, short-range forces such as covalent, ionic, and hydrogen bonds. At

the other extreme, Brownian forces are negligible because the filaments are short (~100 nm) compared to their persistence length ($E_f I/k_b T \approx 3\,\mu m$).

Translocation through the negatively charged arms of the nuclear pore baskets is regulated by electrostatics (Colwell et al., 2010), with time-lapse AFM revealing that the distal ring rotates in response to changes of calcium ion concentration (Panté and Aebi, 1996; Stoffler et al., 1999a). A potential driving force for nuclear basket conformations is therefore the interaction of the cloud of positively charged counter-ions with the spatially distributed electrostatic charges on nuclear basket filament proteins (Zhao et al., 2014) and with NPC proteins such as phenylalanine-glycine nucleoporin (Peyro et al., 2015a, b). We therefore hypothesized that the coiled filamentous structure of the nuclear basket, with its large (~200 kDa) and charged protein arms (Mario et al., 2013; Strambio-De-Castillia et al., 1999), may provide a hypersensitive mechanosensitive gating mechanism for transport of molecules. We asked, what is the selective gating mechanism for transport of large molecules through NPCs, and can stretching of the nuclear envelope affect this?

2. Methods

As NPCs are one of the largest protein complexes within the cell (Apelt et al., 2016; Lim et al., 2006), its dynamics is not well suited to present molecular dynamics simulation techniques. We therefore developed continuum approaches to simulate NPC gated nucleocytoplasmic transport.

2.1. Nuclear membrane mechanics

The nuclear membrane is elastic over the micro- to millisecond timescales of the nuclear basket dynamics and molecular gating, but viscous over the 10-minute and greater timescales of the viscoelastic lamina (Deviri et al., 2017; Kim et al., 2015; Swift et al., 2013b). The boundary conditions on the nuclear membrane insertion of the pore are thus sensitive to the state of stress in the nuclear membrane, and, for sustained loadings such as hypertension, to the history of the state of stress. Because the radius of curvature of the membrane (~microns) is large compared to the diameter of the nuclear basket (~tens of nanometers), the nuclear membrane was treated as a thin, flat annulus subjected to an equibiaxial stress σ_0 within its plane; its upper and lower surfaces were free of mechanical traction. The nuclear membrane insertion of the nuclear basket was thus displaced from its reference state with radius of nuclear pore a_0 and far field stress σ_0 by an amount (Deviri et al., 2017):

$$u_r(r = a_0) = 2a_0\frac{\sigma - \sigma_0}{E} - (1+\nu)\frac{T - T_0}{E} \tag{1}$$

where σ is the far field stress; T is the resultant of line tension (force per unit length) and interaction forces among proteins at the nuclear membrane insertion of the NPC; T_0 is the initial line tension; E (1–150 kPa (Cao et al., 2013)) is the elastic modulus of the nuclear membrane; ν (~0.4 (Chen et al., 2008; Wagner et al., 1999; Wolf and Mofrad, 2008; Zhu et al., 2016)) is its Poisson ratio; $\varepsilon = (1-\nu)\sigma/E$ is the far-field strain.

2.2. Nuclear basket filament kinematics

Nuclear basket filaments were modeled as pinned at the nucleoplasmic and distal rings of NPC (Fig. 1 and Fig. S1). In our coarse-grained simulations, we tracked the sizes of the inter-filament gaps x_{ij} between the midpoints of every pair of filaments i and j. Filaments were treated as inextensible and of length l. The maximum spacing between midpoints was found from the case of fully stretched nuclear basket, with $x_{ij}^{max} = (a+b)\sin\frac{\pi}{8}$ (Fig. 1f) and the minimum was found from the case of a rotation of the basket to the point of steric hindrance, $x_{ij}^{min} = (a-b)\sin\frac{\pi}{8}$ (Fig. 1f), where a is the radius of nucleoplasmic ring (and hence nuclear pore) and b is the radius of distal ring. All other conformations had spacings between these two extremes.

2.3. Nuclear basket and nuclear membrane mechanics

The NPC was coarse-grained into an elastic network with conformations dominated by electrostatic interactions. This is appropriate because the persistence length (quantifying the stiffness of a polymer) of the nuclear basket filaments was an order of magnitude longer than the filament length, meaning that enthalpic terms dominate and a linear elastic formulation is appropriate. The persistence length ($E_f I/k_b T$ (Gittes et al., 1993)) of a nuclear basket filaments was on the order of 3 μm, where $E_f \approx 1$ GPa is the effective elastic modulus of a filament protein, $I = \pi d^4/64 \approx 1.3 \times 10^{-35}$ m^4 is the second moment of the area of a filament of radius d, k_B is Boltzmann's constant, and T is absolute temperature. Thus the persistence length was far larger than the length of a nuclear basket filament.

Estimation of mechanical fields was performed using commercial 3D modeling and stress analysis software (Autodesk Inventor 2017, AutoDesk, USA; and Abaqus 6.14, Dassault, France) using NPC morphology reported in the literature (Kowalczyk et al., 2011; Rout and Aitchison, 2001) (Fig. 1, Table 1) along with reported values of the effective elastic modulus (~100 kPa) and Poisson ratio (~ 0.4) (Chen et al., 2008; Wagner et al., 1999; Wolf and Mofrad, 2008; Zhu et al., 2016) of nuclear basket

Table 1
Physical parameters used in simulations.

Physical parameter	Baseline	Value	References
Radius of nuclear pore/nucleoplasmic ring (a_o)	30 nm	35 nm	Based on Moussavibaygi et al. (2011)
		~35 nm	Based on Rout and Aitchison (2001)
		60 nm	Based on Adams and Wente (2013)
Radius of distal ring (b)	5 nm	~10 nm	Based on Rout and Aitchison (2001)
		15 nm	Based on Adams and Wente (2013)
Length of filaments (l)	60 nm	75 nm	Based on Moussavibaygi et al. (2011)
		~90 nm	Based on Adams and Wente (2013)
Inter-filament gap (x)		20 nm (*Xenopus*)	Based on Rout and Aitchison (2001)
Diameter of filaments (d)	4 nm	4nm (*Xenopus*)	Based on Rout and Aitchison (2001)
Young's modulus of filaments (E)	Rigid	2.2 GPa (by measuring wave speed through actin) 10–69 GPa (equivalent frequency estimate)	Wolf and Mofrad (2008), Zhu et al. (2016)
Relative dielectric constant of bulk solvent (ε)	80	80	At room temperature; varies little except at non-physiologically high salt concentration.
Dielectric permittivity in vacuum (ε_0)	8.85×10^{-12}F/m	8.85×10^{-12}F/m	
Boltzmann constant (k_B)	1.38×10^{-23} J/K	1.38×10^{-23} J/K	
Protonic charge (q)	1.602×10^{-19}C	1.602×10^{-19}C	
Ionic number density (ρ_∞)	1 mM	1 mM	Low salt buffer (1 mM KCl and 10 mM Hepes) (Jarnik and Aebi, 1991; Reichelt et al., 1990; Stoffler et al., 1999b)
Mass of one nuclear basket filament (m)	100 kDa $=1 \times 10^5$g/mol $=6.02 \times 10^{-21}$kg	~100 kDa $=1 \times 10^5$g/mol $=6.02 \times 10^{-21}$kg	Davis (1995)

proteins. Quadratic interpolation finite element analysis was performed, and refinement studies showed numerical convergence with 42,000 nodes and 24,000 10-node quadratic tetrahedral (C3D10) and 8-node linear brick (C3D8R) elements. Simulations were performed on a HP Z820 workstation with 2.6 GHz CPUs and 64 GB RAM.

2.4. Electrostatic interactions of nuclear basket filaments

Electrostatic interactions between nuclear basket filaments were approximated with Ray-Manning type charge condensation (Fig. 1d)(Ray and Manning, 2000). Although many other approaches are reasonable, this is a reasonable model because two conditions are satisfied. The first condition is that electrostatic interactions must be significant over length scales relevant to NPCs. The Bjerrum length estimates the distance between two elementary charges at which the electrostatic interaction is comparable to thermal motion and it is well-known that the Bjerrum length between two elementary charge is 0.7 nm in water. Adopting the idea from Bjerrum and given that the proteins is charged with ~20 electrons (Filoti et al., 2015), the length (λ_B) for neighboring filaments at which electrostatic interaction is comparable to thermal motion was estimated as (Ray and Manning, 2000):

$$\lambda_B = \frac{z^2 q^2}{4\pi\varepsilon\varepsilon_0 k_B T} \approx 280\ nm \tag{2}$$

Low salt buffer (1 mM KCl and 10 mM Hepes) is widely used to keep the *Xenopus* nuclei intact (Jarnik and Aebi, 1991; Reichelt et al., 1990; Stoffler et al., 1999b). For 1 mM KCl, $\rho_i^\infty = 1 \times 10^{-3}\text{mol/L} \times 6.02 \times 10^{23}$, $q = e$, $z_1 = 1$, $z_2 = -1$, $\varepsilon \approx 80$, $k_B = 1.38 \times 10^{-23}$ J/K, $T = 300$K. The Debye screening length was estimated as (Fisher and Levin, 1993; Ray and Manning, 2000):

$$\lambda_D = \left(\sum_i \frac{\rho_i^\infty q^2 z_i^2}{\varepsilon\varepsilon_0 k_B T} \right)^{-1/2} \approx 10\ \text{nm} \tag{3}$$

where ρ_i^∞ is the number density in the bulk solution of ion species i with valence z_i; q is the charge of an electron; ε_0 is the dielectric permittivity in a vacuum; and ε is the relative permittivity. We note that the Debye screening length could

vary significantly with cellular microenvironment, and is sufficiently sensitive to ionic concentrations that it could be used to actively control NPC opening. A physiological range of 0.7–20 nm has been reported in the literature. Ray and Manning estimated the Debye screening length as 3 nm for 10^{-2} M NaCl and 9.6 nm for 10^{-3} M NaCl (Ray and Manning, 2000); Aleksandar et al. estimated the Debye screening length of physiological buffer as ~3–20 nm (Aleksandar et al., 2011); Stern et al. estimated the Debye screening length of PBS solution as 0.7–7.3 nm (Stern et al., 2007). Thus, our estimation of the Debye screening length is within this physiological range.

Both the scale of nuclear basket and the Debye screening length (λ_D) are smaller than the length (λ_B) for neighboring filaments at which electrostatic interaction is comparable to thermal motion, indicating that it is important to consider the effects of electrostatic interactions. Because the Debye screening length is comparable to the size of nuclear basket, charge condensation could affect nuclear basket filament interactions.

The second condition is related to the response time of nuclear basket filaments. The response time related to the rate at which a filament of effective mass m can cross an energy barrier Φ associated with conformational changes, and can be estimated using the impulse momentum relation $p = \sqrt{2m\Phi} = \kappa\Phi t_c$, where $\kappa = \lambda_D^{-1}$ is the Debye screening parameter. Noting that $\Phi = \frac{\lambda_B}{\lambda_D} k_B T$ yields:

$$t_c = \lambda_D \sqrt{\frac{\lambda_D 2m}{\lambda_B k_B T}} \approx 3 \text{ ns} \tag{4}$$

This is far smaller than the millisecond timescale of NPC transport (Moussavibaygi et al., 2011), implying that conformational changes of the nuclear basket are significant on the timescale of transport.

Because of the size difference between the nuclear basket filaments and NPC rings and because of the absence of evidence of high charge density on the rings, our coarse-grained electrostatic model focused on the nuclear basket filaments. The electrostatic energetic state of a configuration was asummed from the interaction energies of each pair of filaments:

$$U = \frac{1}{2} \sum_{i=1}^{7} \sum_{j=i+1}^{8} W\left(x_{ij}\right) \tag{5}$$

where $W(x_{ij})$ represents the interaction energy between a pair of poly-ions i and j of filaments separated by distance x_{ij}. The Ray-Manning form for $W(x_{ij})$ is well approximated by (Fig. 1d, Supplemental Methods):

$$W(x) \approx \begin{cases} E_A \dfrac{c - K_0(\kappa x)}{c - K_0(1/e)}, & \kappa x \le 1/e \\ E_R - (E_R - E_A)\dfrac{1 - \kappa x}{1 - 1/e}, & 1/e < \kappa x \le 1 \\ E_R \dfrac{K_0(\kappa x)}{K_0(1)}, & \kappa x > 1 \end{cases} \tag{6}$$

where E_A is the depth of the attraction potential well, E_R is the height of the energy barrier for charge condensation, c describes the close-proximity repulsion, and K_0 is the zeroeth order Bessel function of the second kind. The Ray-Manning solution provides estimates of the parameters for lines of charge, as described in the Supplemental Methods. We emphasize that we apply the model phenomenologically, and that effects of molecular orientation on the potential function would likely introduce further nonlinearity.

3. Results and discussion

Simulations revealed that nuclear basket filaments could rearrange into configurations with openings them that were sufficiently large to allow passage of proteins whose mean radius exceeds the radius of the distal ring (Fig. 3). The expansion mode, in which the filaments were radial, represented the upper limit for interaction energy. The torsional mode, with filaments slightly inclined, corresponded to attractive filament interactions. Cross and spiral modes corresponded to lower limits of interaction energies. In the cross mode, the filaments were perpendicular to both rings and crossed at an intersection point. In the spiral mode, the nuclear basket stretched to a planar configuration with a spiral as filaments attracted one other. Bi-stability was possible between the expansion mode and the three other modes.

The five factors that defined the gating function of the nuclear basket were the Debye screening length $1/\kappa$; the radius a of the nucleoplasmic ring; the radius b of the distal ring; and the length l and diameter d of the nuclear basket filaments. The Debye screening length $1/\kappa$ was used to normalize all other parameters (a, b, l and d) in the figures. We chose a as the independent variable for Figs. 4, because the radius a of the nucleoplasmic ring bridged the membrane strain and the geometrical factors (*cf.* Fig. 2). d had only minor influence on the results (see Supplementary Material), but varying the parameters l and b gave rise to a variety of patterns (Figs. 5 and 6). Simulations revealed that nuclear basket filaments could rearrange into configurations with openings that were sufficiently large to allow passage of proteins whose mean radius exceeds the radius of the distal ring. To estimate the size of a protein that could pass through these “transverse pores” (see supplementary materials), we calculated the radius r of the largest sphere that could pass through each configuration of nuclear basket filaments (*cf.* Fig. 1f).

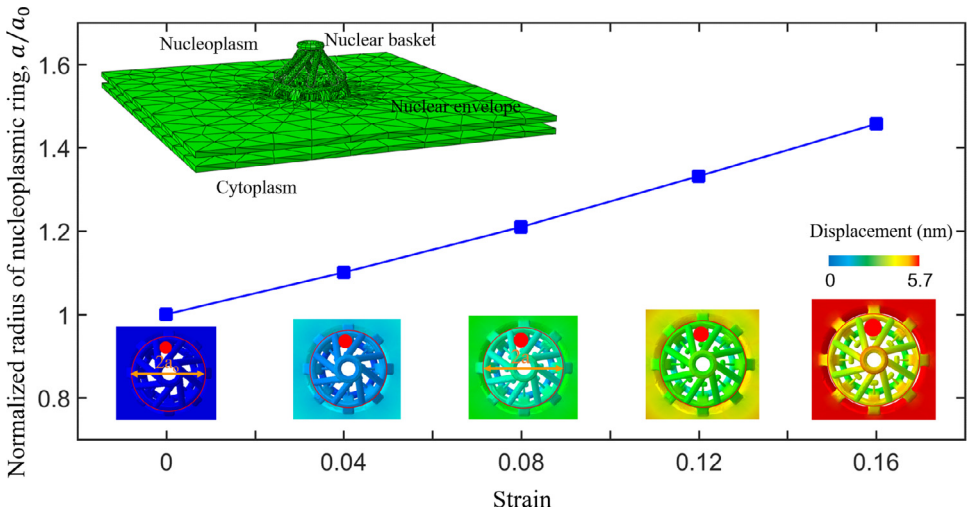

Fig. 2. The nuclear basket responded to nuclear membrane strain by untwisting. Mechanical analysis of a fictional nuclear basket having no electrostatic interactions showed that this torsional opening enabled increasingly large spheres (molecules) to pass through transverse pores that opened between the nuclear basket filaments.

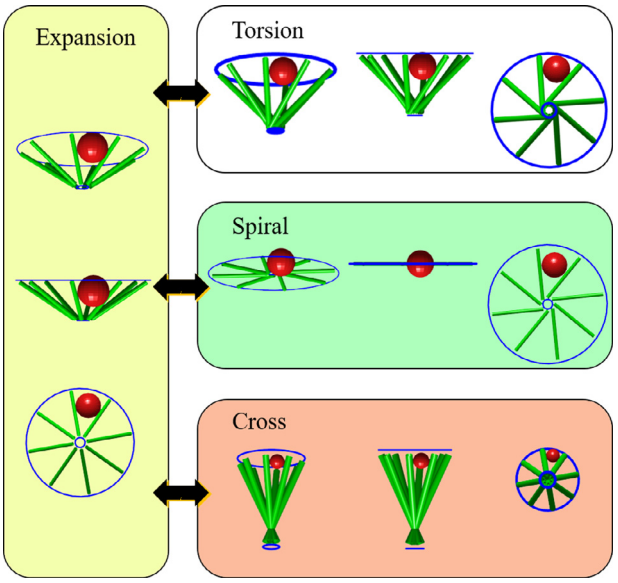

Fig. 3. Four classes of opening modes were observed in the nuclear basket. The expansion mode, in which the filaments were radial, represented the upper limit for interaction energy. The torsional mode, with filaments slightly inclined, corresponded to attractive filament interactions. Cross and spiral modes corresponded to lower limits of interaction energies. In the cross mode, the filaments were perpendicular to both rings and crossed at an intersection point. In the spiral mode, the nuclear basket stretched to a planar configuration with a spiral as filaments attracted one other. Bi-stability was possible between the expansion mode and the three other modes.

3.1. Stretching of the nuclear membrane tends to untwist the nuclear basket and widen transverse nuclear basket pores

We first studied a fictional nuclear basket having no electrostatic interactions between the basket filaments (inset, Fig. 2). To assess both the structural resistance of the NPC relative to the nuclear membrane and the degree to which the filaments could be modeled as rigid rods, the entire basket structure was treated as linear and isotropic. As the nuclear membrane stretched, the basket filaments untwisted (Supplemental Video S1), consistent with the proposed iris-like diaphragm model of opening (Stoffler et al., 1999a). This opening enabled increasingly large spheres (*i.e.*, molecules) to pass through the transverse pores (Fig. 2), consistent with observations that gaps between filaments can exceed the diameter of the distal ring under certain conditions (Arlucea et al., 1998; Lim et al., 2006).

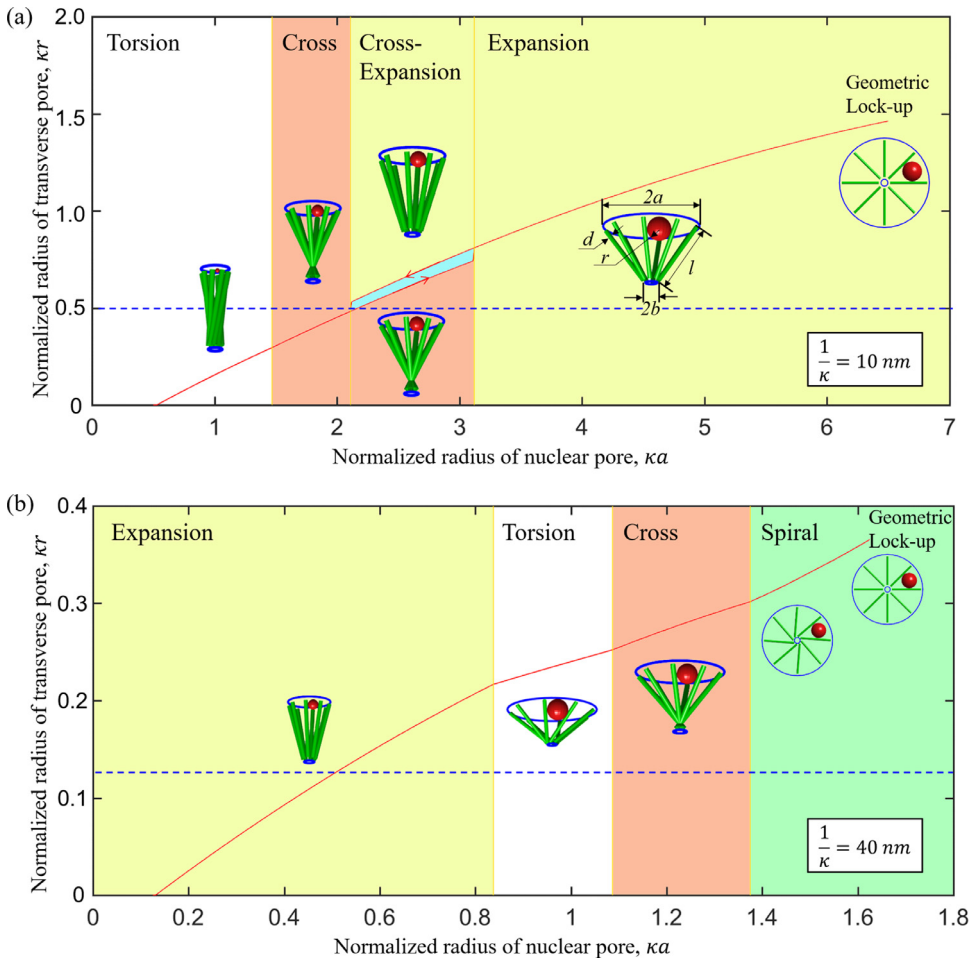

Fig. 4. Electrostatic interactions enabled mechanosensitive transitions of nuclear basket conformations. Nuclear membrane stretch was modeled by varying the dimensionless nucleoplasmic ring radius, $\boldsymbol{\kappa a}$, while maintaining all other parameters at the levels appropriate for the *Xenopus* nuclear basket ($b =$ 5nm, $l = 60$nm, $d = 4$nm, Table 1). Conformations and the transitions between them were governed by κa (Video S2). (a) For $1/\kappa = 10$ nm, the normalized radius of transverse pore (κr) increased with the normalized radius (κa) of the nuclear pore. (b) For $1/\kappa = 40$nm, representing a change in electrostatic environment, the bi-stable region evident in (a) vanished, comfirming the importance of electrostatic regulation on nuclear basket conformations. Blue dash lines represent radius of the normalized radius of distal ring κb. (For interpretation of the references to colour in this figure legend, the reader is referred to the web version of this article.)

The membrane insertion and nuclear basket filaments deformed extensively in response to membrane stretch, but the weak flexural resistance of the filaments transferred little stress to the distal ring, which remained relatively rigid (Fig. S2). NPCs provided little resistance to the expansion of nuclear pore except at very high levels of strain (Fig. S3). Thus, membrane stretch could be approximated as producing a radial displacement of the nucleoplasmic ring in the subsequent simulations, and the long nuclear basket filaments could be approximated as rigid, hinged rods connecting to a rigid distal ring.

3.2. Electrostatic interactions are a dominant force driving NPC basket filament conformations

Although deformation of the membrane dominated the distortion of the nucleoplasmic ring, electrostatic interactions amongst nuclear basket filaments dominated the conformations of nuclear basket filaments between the nucleoplasmic ring and the distal ring. The transformations between these conformations were governed by the dimensionless ratio κa of the nuleoplasmic ring radius a to the Debye screening length $1/\kappa$. The Debye screening parameter κ varies with the ionic strength of the nucleoplasm.

In Fig. 4, plotted for *Xenopus*, nuclear membrane stretch was modeled by varying the nucleoplasmic ring radius a as an independent variable, while maintaining the distal ring radius b, the filament length l and the diameter d. To model responses to changes in ionic strength, two different values of the Debye screening length $1/\kappa$ were studied, with κ in Fig. 4(b) 1/4 of that in Fig. 4(a). The Debye screening length, is influenced by the number density of ions in the bulk

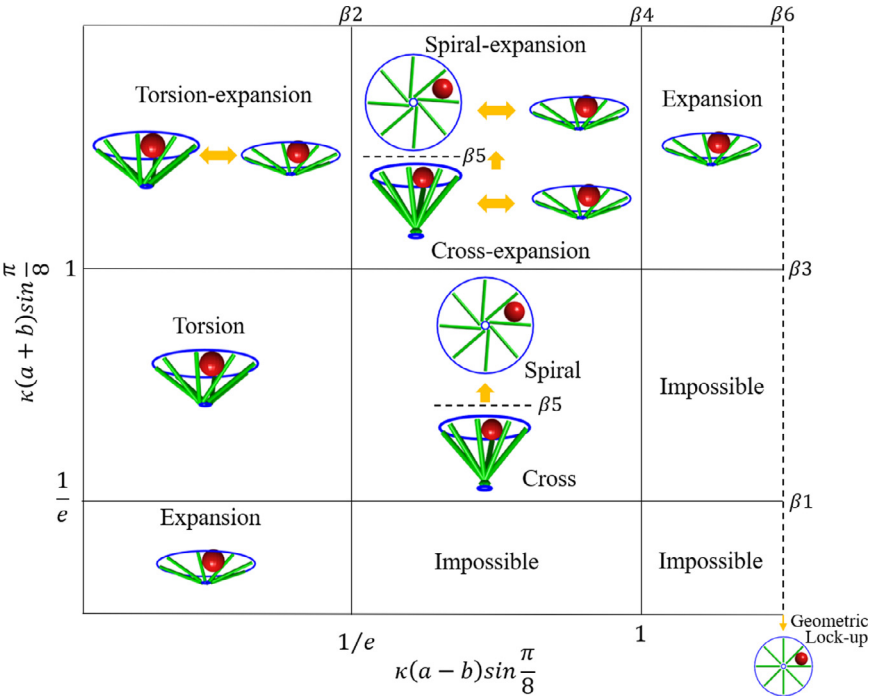

Fig. 5. Phase diagram of nuclear basket conformations. The phase space constitutes the normalized lower (horizontal axis) and upper (vertical axis) limits of center-to-center spacings between nuclear basket filaments. Torsion-expansion, spiral-expansion and cross-expansion modes were bi-stable combinations of two modes. Note that the locations of dashed lines $\beta 5$ and $\beta 6$ vary with κ.

solution (Fisher and Levin, 1993; Ray and Manning, 2000), and indeed nuclear basket conformations have been reported to change in response to Ca^{2+} changes (Panté and Aebi, 1996; Stoffler et al., 1999a). The bi-stable region vanished in Fig. 4(b), comfirming the importance of electrostatic regulation on nuclear basket conformations.

With large κa (Fig. 4a), as occurs with relatively weak electrostatic interactions, the nuclear basket adopted the torsional opening mode seen in our full continuum simulations with no electrostatic interactions (*cf.* Fig. 2). This enabled the largest molecules to pass through the putative transverse pore of the NPC. With κa decreasing to the range of $2.1 \leq \kappa a \leq 3.1$, electrostatic attraction increased and a bifurcated region developed, with two configurations of equal energy, *i.e.*, a torsional opening mode and a crossed configuration. The crossed configuration closed the channel that transports molecules through the distal ring, and slightly decreased the size of the molecule that could traverse the transverse pore. Below κa=2.1, only the crossed configuration was favored energetically, and below $\kappa a \approx 1.5$, the maximum hard sphere radius of a molecule that could cross the transverse pore dropped below the radius of the distal ring. The size range of molecules that could be transported through the NPC was up to ~25–50 nm in diameter, comparable to observations of transported cargo-receptor-gold complexes (Panté and Kann, 2002).

It should be noted that the Debye screening length could vary significantly with cellular microenvironment. In Fig. 4(b), κ is reduced to one fourth of those in Fig. 4(a), which could be interpreted as the change in electrostatic environment. General trends remained the same, but the bifurcated region was lost (Fig. 4). Fig. 4(b) could also be considered as a hypothetical nuclear basket with filaments that were one fourth the length but had identical slenderness ratios. Because the diversity of diameters and lengths of nuclear basket filaments is unknown, it could also show how variations to filament dimensions affect gating. Increasing only the thickness of the filaments provided steric restriction against the passage of larger molecules, but again retained the general trends (Fig. S4a). The exception was that sufficiently thick filaments precluded the existence of the bifurcated region of κa. Further variations of parameters enabled extension of the bifurcated region of κa, and also introduced a family of new bifurcations (Fig. S4b).

Bifurcation was possible when the interactions could switch from attractive to repulsive for configurations within the steric limits: *i.e.* $\kappa(a-b)\sin\frac{\pi}{8} < 1 < \kappa(a+b)\sin\frac{\pi}{8}$ (Fig. 5). In such a case, both the upper and lower limits were stable. These bifurcations could act as a switch for the central portal through the nuclear basket. Electrostatic interactions in such a state could therefore cause the nuclear basket to function as a bi-stable switch.

While in the state in which the nuclear basket could serve as a bi-stable switch for the central portal, the transverse pore size changed relatively little. For a typical *Xenopus* nuclear basket, with geometrical parameters listed in Table 1, the gap was roughly 1.2 nm. This was in contrast to other regions of phase space, in which the transverse pore was sufficiently large to facilitate the translocation of large molecule. For a typical *Xenopus* nuclear basket, the transverse pore could be two times larger than the central portal (Fig. 4).

3.3. Membrane mechanics, ionic concentrations, and geometrical factors collectively control the mechanosenstivity of NPC gating

Our analyses revealed that nuclear basket conformations were controlled by both mechanical and ionic factors. The mechanical factors entered the model through the radius of the nucleoplasmic ring, a, which increased with increasing nuclear membrane tension. The ionic factors entered the model through the Debye screening length, $1/\kappa$, which decreased with increasing ionic concentrations. These factors, combined with the geometrical structure of the NPC baskets, led to certain NPC configurations favored under specific mechanical and ionic conditions.

We began by studying the two governing dimensionless parameters that emerged from the solution: $\bar{x}_{min} \equiv \kappa(a-b)\sin\frac{\pi}{8}$ and $\bar{x}_{max} \equiv \kappa(a+b)\sin\frac{\pi}{8}$ (Fig. 5). $\bar{x}_{min}$ corresponded to the minimum geometrically allowable center-to-center spacing of nuclear basket filaments, normalized by κ, and $\bar{x}_{max}$ corresponded to the maximum. When $\bar{x}_{max}$ and $\bar{x}_{min}$ were both small (<1/e) or both large (>1), the nuclear basket responded to stretch via pure expansion (Fig. 5). When $\bar{x}_{min}$ was small (<1/e) and $\bar{x}_{max}$ was intermediate ($1/e \leq \bar{x}_{max} \leq 1$), the torsional opening mode representative of weak electrostatic interactions dominated. As $\bar{x}_{max}$ became large when $\bar{x}_{min}$ was small, expansion became another stable state besides torsion as the membrane stretched. Intermediate levels of $\bar{x}_{min}$ gave rise to the greatest diversity of opening modes (middle row, Fig. 5).

Switching amongst the states in Fig. 5 exhibited mechanosensitivity and ionic sensitivity. As will be discussed below, the greatest mechanosensitivity arose for intermediate values of $\bar{x}_{min}$. For large $\bar{x}_{max}$ within this range, mechanosensitivity was achieved through transition from spiral to expansion modes (for $a+b>l$), or from transition from crossed-filament to expansion modes ($a+b<l$) (Fig. 5). For intermediate $\bar{x}_{min}$ and $\bar{x}_{max}$, mechanosensitivity was achieved through transition from crossed-filament to spiral modes with increasing nuclear membrane stretch.

To further explore how changes to mechanics and ionic concentrations affected NPC gating, we plotted these states and the size of the transverse pore as a function of the normalized sizes of the nucleoplasmic (κa) and distal (κb) pores (Fig. 6). Mechanical effects were evident as horizontal shifts in Fig. 6 (changes to κa), and ionic effects were evident as diagonal shifts associated with changes to the Debye screening parameter, κ. The phase boundaries of Fig. 5 mapped onto the κa-κb phase diagram of Fig. 6a as a series of diagonal lines. Sharp jumps in the size of the transverse pore were evident at these boundaries, and, for intermediate values of κa, bifurcation-based gating cycles were possible, in which relatively small changes to nuclear membrane stretch could increase the transverse pore size by an order of magnitude. These regions indicated sets of mechanical and ionic conditions for which the NPC configurations could be expected to be highly sensitive to mechanical perturbations.

Because the variability of the size and shape of nuclear baskets is not yet known either within a single cell or across cell types or species, we next asked how differences in the length l of nuclear basket filaments might affect conformations and their sensitivity to their ionic environment. These were studied through a phase diagram analogous to that of Fig. 6a, but now with and the dimensionless filament length κl on the vertical axis (Fig. 6b). Bifurcation-based gating cycles were possible as the nuclear basket shifted from the crossed-filament configuration to the torsional configuration (Supplemental Movies 1 and 2) in the bifurcation zone of the phase diagram (bounded by lines $\beta 3$ and $\beta 5$). The size of the transverse pore was relatively independent of κl beyond a threshold (line $\beta 6$ in Fig. 5). Similar trends were evident on a phase diagram of κd and κa (Fig. S6).

The predicted conformational bifurcations provided a mechanism by which small perturbations to ionic concentrations and membrane tension could be amplified into significant changes in gating behavior. These regions were evident in Figs. 5, 6a,b and 7 as sudden changes in transverse pore size associated with bistability of the pores, and arose when electrostatic interactions could switch from attractive to repulsive for configurations within the steric limits: *i.e.* $\kappa(a-b)\sin\frac{\pi}{8} < 1 < \kappa(a+b)\sin\frac{\pi}{8}$. In such cases, both the upper and lower limits were stable, and hypersensitivity to membrane tension could enable switching between the two limits.

The physics underlying these switching behaviors was an interplay between the electrostatic energy potential and the geometry, especially the steric limits. This gave rise to transformations of stable states, including bifurcations (Supplemental Video S1). Bifurcations arose when the minimum energy configuration (*cf.* Fig. 1d) would fall outside of the steric limits if those were possible. In these conditions, stable states existed on either side of the minimum energy configuration, leading to bifurcated regimes of two kinds. In the first, the Debye screening length was small compared to the geometrical dimensions. In this case, configurations corresponding to the energy well and the energy barrier (Fig. 1d) were possible within the steric limits, and the "closed" torsional mode, in which the nuclear basket arms had center-to-center spacing near $1/\kappa$e, had energy very near that the "open" expansion mode, in which the nuclear basket arms were spread far apart (Fig. 5, Torsion-Expansion mode).

In the second case, the Debye screening length was large compared to the geometrical dimensions. In this case, a bi-stable state existed in which configurations associated with the energy barrier were within the steric limit. Here, both the shortest and the longest distance between filaments could be favored energetically (Fig. 5, Cross-Expansion mode and Spiral-Expansion mode).

In both cases, because the two stable configurations were separated by an energy barrier, bi-stable switching could occur. The previous history of mechanical loading is important, because energy must be available to enable a NPC to transition from an initial configuration to the alternative configuration, leading to a transformational directionality. For example (Fig. 4), as the cytoplasmic ring enlarged, transforming from the torsion mode to the cross mode and then further into the cross-expansion regime, the cross mode would be expected to be favored initially, and snap-through to expansion mode would be expected when the cross mode passed out of the steric limits. Similarly, a subsequent reduction in membrane tension

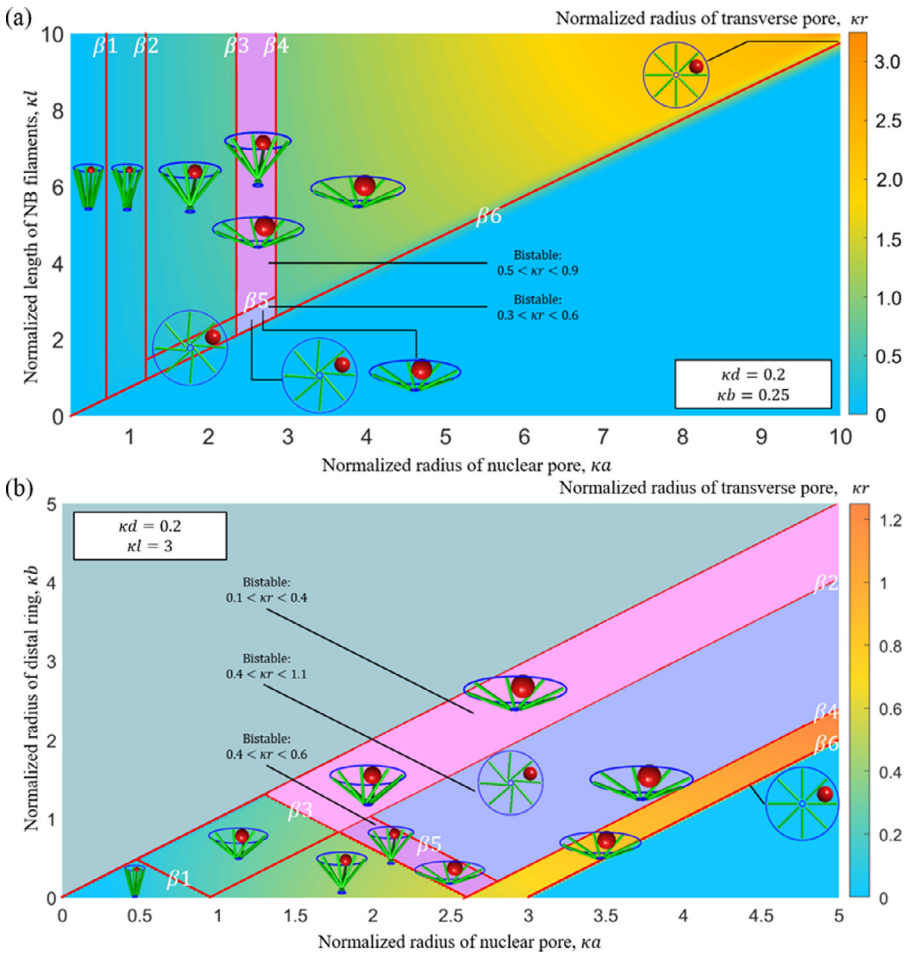

Fig. 6. Local ionic concentrations, represented by the Debye screening parameter, κ, and the membrane tension, represented by the tension-dependent nucleoplasmic ring radius, a, combined with geometrical parameters of the nuclear basket determine switching behavior and the size of the transverse pore. (a) For all plausible radii of the distal ring, b, the minimum energy NPC configurations could vary with the degree to which the nucleoplasmic ring was stretched by membrane tension. For certain values of κb, bifurcation-based gating cycles were possible, in which relatively small changes to nuclear membrane stretch could increase the transverse pore size by an order of magnitude. This occurred as the nuclear basket shifted from the crossed-filament configuration to the torsional configuration. Note that this phase diagram is symmetrical with respect to the line $a = b$, but solutions with $b > a$ (gray region) are not meaningful. (b) Different bifurcation-based gating cycles were possible for nuclear baskets with arms of different lengths l, suggesting that further tuning of NPC mechanoresponsiveness would be possible for nuclear baskets of different size. In panel (b), only cases of $a < l$ were considered. In both panels, the boundary lines are the following: $\beta1$: $\kappa(a+b)\sin\frac{\pi}{8} = 1/e$; $\beta2$: $\kappa(a-b)\sin\frac{\pi}{8} = 1/e$; $\beta3$: $\kappa(a+b)\sin\frac{\pi}{8} = 1$; $\beta4$: $\kappa(a-b)\sin\frac{\pi}{8} = 1$; $\beta5$: $a+b=l$; $\beta6$: $a-b=l$. These boundaries correspond to those in Fig. 5.

and cytoplasmic ring radius would initially favor expansion mode, and until the expansion mode was no longer within the steric limits.

3.4. Model predictions unify the range of available observations

Most descriptions of the nuclear basket report axisymmetric deformation (Ma and Lippincott-Schwartz, 2010; Moussavibaygi et al., 2011; Rout and Aitchison, 2001; Solmaz et al., 2011), which is consistent with the expansion mode we observed here. However, rotationally symmetrical nuclear basket motions have been observed (Akey and Radermacher, 1993; Garcia et al., 2016; Rout and Aitchison, 2001; Yang et al., 1998), consistent with the torsional mode we observed here. Calcium-dependent, “iris-like” (rotationally symmetric) distal ring opening and closure observed by time-lapse AFM (Panté and Aebi, 1996; Stoffler et al., 1999a) is consistent with closure mode we observed here in which charge condensation induced crossing of the nuclear basket filaments. The crossed-filament to expansion mode transition was predicted in our simulations to occur near κa=3. Both of these conformations have been observed simultaneously in a *Xenopus* oocyte nucleus (Arlucea et al., 1998; Stoffler et al., 1999a), consistent with our observation that a bifurcation is possible under certain conditions of membrane stretch and Debye screening (Figs. 4–6). Using this as a guide, we predict that the Debye screening length of a

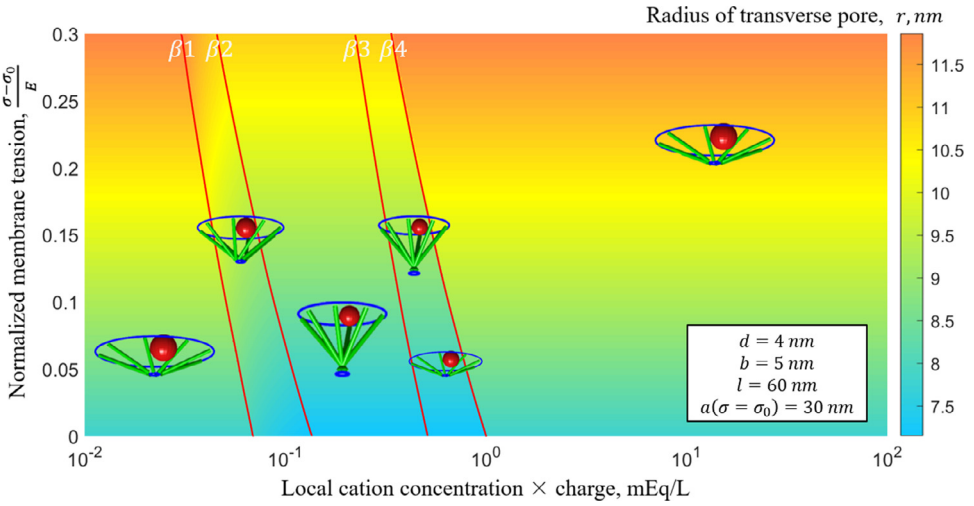

Fig. 7. Nuclear ionic concentrations and membrane tension governed nuclear basket configurations. Here, $d = 4$nm, $b = 5$nm, $l = 60$nm and $a = 30$nm when the membrane was in the reference state with stress σ_0. In calculating the Debye screening length, ions were treated as be monovalent. Boundaries $\beta 1 - 4$ were as in Figs. 5 and 6. $\beta 5 - 6$ were not plotted because they were not within the physiological range for the specific parameters chosen. In the case of bi-stable states, the background shading patches represented the radius of the smaller of the two possible transverse pore sizes. The sharp change of transverse pore size indicated the mechanosensitivity of gating.

nuclear basket filament is on the order of $1/\kappa \sim 20$nm for a 60 nm nucleoplasmic ring, which is a reasonable value (Ray and Manning, 2000).

Given these observations, we return to the question of how large molecules might pass through the NPC. The dominant hypothesis is that the distal ring of the nuclear basket must stretch to accommodate large molecules (Arlucea et al., 1998; Kramer et al., 2008; Sakiyama et al., 2017), but our continuum simulations suggest that this is unlikely. Instead, our simulations suggest that the distal ring is relatively stiff, and that the combination of membrane kinematics and electrostatically-driven conformational dynamics enables large molecule transport through a mechanosensitive transverse pore.

The simulations showed several modes of deformation that have not yet been observed, but these provide targets for future experimental searches for mechanically-driven responses under conditions of large nuclear envelope strain.

3.5. The proposed transverse NPC ports provide a possible mechanism for nuclear mechanotransduction

When applied to a specific cell, *e.g.*, a *Xenopus* oocyte, without normalization by the Debye screening parameter, the boundaries between modes of opening seen in Figs. 5 and 6 became curved (Fig. 7). Here, the effect of ionic concentration was represented by the charge (horizontal axis), and the effects of membrane stress were represented by an effective strain that was linearly proportional to membrane stress (vertical axis). Although the rupture strain of a *Xenopus* oocyte nucleus is not known, data for osmotic rupture of the entire oocyte suggest that a strain of 10–20% might be a reasonable range (Preston et al., 1992). Because this range could extend dramatically with wrinkling of the membrane, a larger range of strains were included on the vertical axis. Across the entire range of cation concentrations, mechanosensitivity was enabled. Around $\sim$1 mEq/L (to the right of line $\beta 3$), mechanosensitivity was enhanced by bistable switching.

A key question in mechanotransduction is whether deformation of the nucleus can affect gene expression and protein translation. Our results predicted that the membrane stretch can change the radius of the nucleoplasmic ring of NPCs, and that electrostatic can change nuclear basket conformations. These conformational changes can fully block the central nuclear pore channel, or open transverse pores that enable passage of molecules larger than the diameter of the NPC distal ring. Although these potential pathways are not required for proteins such as YAP and TAZ in the hippo pathway, which are sufficiently small to pass through the distal ring, they provide a potential mechanism for increased rates of translocation and for translocation of larger molecules. This mechanism for larger molecule transport might relate to observations of how lamin-B elasticity affects nuclear transport, and also of how long-term deformation of viscoelastic lamin-A might enable nuclear mechanotransduction of long-term mechanical loads such as those associated with hypertension (Bhattacharjee et al., 2013; Buxboim et al., 2017; Dahl et al., 2004; Swift et al., 2013a). The presence of large reservoirs of calcium ions in the endoplasmic reticulum surrounding NPCs suggests a mechanism by which the Debye screening length could be modified in the vicinity of an NPC, further enhancing mechanosensitivity. The existence of bi-stable switching over certain conditions provides a possible mechanism for hyper-sensitivity of NPCs to mechanical stretch.

4. Conclusions

Our simulations suggested two mechanisms for mechanosensitive, gated transport through the NPCs. Both were activated by membrane stretch in conjunction with electrostatic interactions between nuclear basket filaments. The first involved transport through the distal ring, transport that could be obstructed by electrostatic closure of nuclear basket filaments. The second involved transport through the nuclear basket itself, enabling transport of large molecules through pores that arose between the nuclear basket filaments. Through a trade-off between membrane stretch and electrostatic attraction, the sizes and presumably electrostatic landscape of these transverse pores were highly sensitive to the mechanical state of the nucleus. Under certain conditions NPCs could act as bi-stable switches. Our results suggested a selective transport mechanism that arose from coupled effects of mechanical stretch and electrostatic force. As the cytoplasmic ring radius a changed in response to mechanical stretch of the nuclear membrane, conformations could change in a way that depended upon the electrostatic environment, as quantified by the Debye screening parameter, κ. Changes to either of these could change NPC gating, and furthermore tune the gates to become hypersensitive to membrane stretch through configurational bifurcations.

Author contributions

S.B.L. and H.Q.Y. developed the mechanical model of NPC and performed the numerical simulations. G.M.G. supervised the simulation work. F.X. and T.J.L. initiated and supervised the project. All authors discussed the results and contributed to writing the manuscript.

Declaration of Competing Interest

The authors declare no competing interests.

Acknowledgments

This work was funded by the National Natural Science Foundation of China (11522219, 11532009, 11902155, 11972280), by the New Faculty Foundation of NUAA(1001-YAH19016), by the foundation of "Jiangsu Provincial Key Laboratory of Bionic Functional Materials" (1001-XCA1816310), by Foundation for the Priority Academic Program Development of Jiangsu Higher Education Institutions, by the National Science Foundation through the Science and Technology Center for Engineering Mechanobiology (CMMI 1548571), and by the National Institutes of Health through grant U01EB016422. We thank an anonymous reviewer for helpful suggestions on presentation of the results.

Supplementary materials

Supplementary material associated with this article can be found, in the online version, at doi:10.1016/j.jmps.2019.103705.

References

Adams, R.L., Wente, S.R., 2013. Uncovering nuclear pore complexity with innovation. Cell 152, 1218–1221.
Akey, C.W., Radermacher, M., 1993. Architecture of the xenopus nuclear pore complex revealed by three-dimensional cryo-electron microscopy. J. Cell Biol. 122, 1–19.
Aleksandar, V., Criscione, J.M., Rajan, N.K., Eric, S., Fahmy, T.M., Reed, M.A., 2011. Determination of molecular configuration by debye length modulation. J. Am. Chem. Soc. 133, 13886–13889.
Apelt, L., Knockenhauer, K.E., Leksa, N.C., Benlasfer, N., Schwartz, T.U., Stelzl, U., 2016. Systematic protein-protein interaction analysis reveals intersubcomplex contacts in the nuclear pore complex. Mol. Cell. Proteomics, 054627 Mcp 15, mcp.M115.
Arlucea, J., Andrade, R., Alonso, R., Aréchaga, J., 1998. The nuclear basket of the nuclear pore complex is part of a higher-order filamentous network that is related to chromatin. J. Struct. Biol. 124, 51–58.
Bhattacharjee, P., Banerjee, A., Banerjee, A., Dasgupta, D., Sengupta, K., 2013. Structural alterations of Lamin A protein in dilated cardiomyopathy. Biochemistry 52, 4229–4241.
Burns, L.T., Wente, S.R., 2014. From hypothesis to mechanism: uncovering nuclear pore complex links to gene expression. Mol. Cell. Biol. 34, 2114–2120.
Buxboim, A., Irianto, J., Swift, J., Athirasala, A., Shin, J.W., Rehfeldt, F., Discher, D.E., 2017. Coordinated increase of nuclear tension and lamin-A with matrix stiffness out-competes Lamin-B Receptor which favors soft tissue phenotypes. Mol. Biol. Cell 28, 3333.
Cao, G., Jie, S., Sun, S., 2013. Evaluating the nucleus effect on the dynamic indentation behavior of cells. Biomech. Model. Mechanobiol. 12, 55.
Cao, X., Ban, E., Baker, B.M., Lin, Y., Burdick, J.A., Chen, C.S., Shenoy, V.B., 2017. Multiscale model predicts increasing focal adhesion size with decreasing stiffness in fibrous matrices. Proc. Natl. Acad. Sci. U. S. A. 114, E4549.
Chen, X., Cui, Q., Tang, Y., Yoo, J., Yethiraj, A., 2008. Gating mechanisms of mechanosensitive channels of large conductance, I: a continuum mechanics-based hierarchical framework. Biophys. J. 95, 563–580.
Colwell, L.J., Brenner, M.P., Ribbeck, K., 2010. Charge as a selection criterion for translocation through the nuclear pore complex. PLoS Comput. Biol. 6, e1000747.
Crisp, M., Liu, Q., Roux, K., Rattner, J.B., Shanahan, C., Burke, B., Stahl, P.D., Hodzic, D., 2006. Coupling of the nucleus and cytoplasm: role of the LINC complex. J. Cell Biol. 172, 41–53.
Dahl, K.N., Kahn, S.M., Wilson, K.L., Discher, D.E., 2004. The nuclear envelope lamina network has elasticity and a compressibility limit suggestive of a molecular shock absorber. J. Cell. Sci. 117, 4779–4786.
Davis, L.I., 1995. The nuclear pore complex. Annu. Rev. Biochem. 1, 865–896.

Deviri, D., Discher, D.E., Safran, S.A., 2017. Rupture dynamics and chromatin herniation in deformed nuclei. Biophys. J. 113, 1060–1071.
Dupont, S., Morsut, L., Aragona, M., Enzo, E., Giulitti, S., Cordenonsi, M., Zanconato, F., Digabel, J.L., Forcato, M., Bicciato, S., 2011. Role of YAP/TAZ in mechanotransduction. Nature 474, 179–183.
Elosegui-Artola, A., Andreu, I., Aem, B., Lezamiz, A., Uroz, M., Kosmalska, A.J., Oria, R., Kechagia, J.Z., Rico-Lastres, P., Le, R.A., 2017. Force triggers YAP nuclear entry by regulating transport across nuclear pores. Cell 171, 1397.
Engler, A.J., Sen, S., Sweeney, H.L., Discher, D.E., 2006. Matrix elasticity directs stem cell lineage specification. Cell 126, 677.
Filoti, D.I., Shire, S.J., Yadav, S., Laue, T.M., 2015. Comparative study of analytical techniques for determining protein charge. J. Pharm. Sci. 104, 2123–2131.
Fisher, M.E., Levin, Y., 1993. Criticality in ionic fluids: Debye–Hückel theory, Bjerrum, and beyond. Phys. Rev. Lett. 71, 3826–3829.
Gallardo, P., Salaspino, S., Daga, R.R., 2017. A new role for the nuclear basket network. Microb. Cell 4, 423–425.
Garcia, A., Rodriguez Matas, J.F., Raimondi, M.T., 2016. Modeling of the mechano-chemical behaviour of the nuclear pore complex: current research and perspectives. Integr. Biol. 8, 1011–1021.
Ghavami, A., Veenhoff, L.M., Van, d.G.E., Onck, P.R., 2014. Probing the disordered domain of the nuclear pore complex through coarse-grained molecular dynamics simulations. Biophys. J. 107, 1393–1402.
Gittes, F., Mickey, B., Nettleton, J., Howard, J., 1993. Flexural rigidity of microtubules and actin filaments measured from thermal fluctuations in shape. J. Cell Biol. 120, 923–934.
Jamali, T., Jamali, Y., Mehrbod, M., Mofrad, M.R., 2011. Nuclear pore complex: biochemistry and biophysics of nucleocytoplasmic transport in health and disease. Int. Rev. Cell Mol. Biol. 287, 233.
Jarnik, M., Aebi, U., 1991. Toward a more complete 3-D structure of the nuclear pore complex. J. Struct. Biol. 107, 291–308.
Kim, D.H., Li, B., Si, F., Phillip, J.M., Wirtz, D., Sun, S.X., 2015. Volume regulation and shape bifurcation in the cell nucleus. J. Cell. Sci. 128, 3375–3385.
Kowalczyk, S.W., Kapinos, L., Blosser, T.R., Magalhães, T., Van, N.P., Lim, R.Y., Dekker, C., 2011. Single-molecule transport across an individual biomimetic nuclear pore complex. Nat. Nanotechnol. 6, 433–438.
Kramer, A., Liashkovich, I., Oberleithner, H., Ludwig, S., Mazur, I., Shahin, V., 2008. Apoptosis leads to a degradation of vital components of active nuclear transport and a dissociation of the nuclear lamina. Proc. Natl. Acad. Sci. U.S.A. 105, 11236.
Lim, R.Y.H., Aebi, U., Stoffler, D., 2006. From the trap to the basket: getting to the bottom of the nuclear pore complex. Chromosoma 115, 15.
Lord, C.L., Timney, B.L., Rout, M.P., Wente, S.R., 2015. Altering nuclear pore complex function impacts longevity and mitochondrial function in S. cerevisiae. J. Cell Biol. 208, 729–744.
Ma, J., Lippincott-Schwartz, J., 2010. Three-dimensional distribution of transient interactions in the nuclear pore complex obtained from single-molecule snapshots. Proc. Natl. Acad. Sci. U.S.A. 107, 7305.
Makhija, E., Jokhun, D.S., Shivashankar, G.V., 2016. Nuclear deformability and telomere dynamics are regulated by cell geometric constraints. Proc. Natl. Acad. Sci. U. S. A. 113.
Mario, N., Molloy, K.R., Rosemary, W., Farr, J.C., Meinema, A.C., Nicholas, V., Cristea, I.M., Chait, B.T., Rout, M.P., Caterina, S.D.C., 2013. The nuclear basket proteins Mlp1p and Mlp2p are part of a dynamic interactome including Esc1p and the proteasome. Mol. Biol. Cell 24, 3920.
Meng, Z., Qiu, Y., Lin, K.C., Kumar, A., Placone, J.K., Fang, C., Wang, K.C., Lu, S., Pan, M., Hong, A.W., 2018. RAP2 mediates mechanoresponses of the Hippo pathway. Nature 560, 655.
Moussavibaygi, R., Jamali, Y., Karimi, R., Mofrad, M.R., 2011. Biophysical coarse-grained modeling provides insights into transport through the nuclear pore complex. Biophys. J. 100, 1410.
Nathan, A.S., Baker, B.M., Nerurkar, N.L., Mauck, R.L., 2011. Mechano-topographic modulation of stem cell nuclear shape on nanofibrous scaffolds. Acta Biomater. 7, 57.
Panté, N., Aebi, U., 1996. Molecular dissection of the nuclear pore complex. Crit. Rev. Biochem. Mol. Biol. 31, 153–199.
Panté, N., Kann, M., 2002. Nuclear pore complex is able to transport macromolecules with diameters of about 39nm. Mol. Biol. Cell 13, 425–434.
Peyro, M., Soheilypour, M., Ghavami, A., Mofrad, M.R., 2015a. Nucleoporin's like charge regions are major regulators of FG coverage and dynamics inside the nuclear pore complex. PLoS One 10, e0143745.
Peyro, M., Soheilypour, M., Lee, B.L., Mofrad, M.R., 2015b. Evolutionarily conserved sequence features regulate the formation of the FG network at the center of the nuclear pore complex. Sci Rep 5, 15795.
Poleshko, A., Shah, P.P., Gupta, M., Babu, A., Morley, M.P., Manderfield, L.J., Ifkovits, J.L., Calderon, D., Aghajanian, H., Sierra-PagÃn, J.E., 2017. Genome-Nuclear lamina interactions regulate cardiac stem cell lineage restriction. Cell 171, 573–587.
Preston, G.M., Carroll, T.P., Guggino, W.B., Agre, P., 1992. Appearance of water channels in Xenopus oocytes expressing red cell CHIP28 protein. Science 256, 385–387.
Ray, J., Manning, G.S., 2000. Formation of loose clusters in polyelectrolyte solutions. Macromolecules 33, 2901–2908.
Reichelt, R., Holzenburg, A., Buhle, E.L., Jarnik, M., Engel, A., Aebi, U., 1990. Correlation between structure and mass distribution of the nuclear pore complex and of distinct pore complex components. J. Cell Biol. 110, 883–894.
Rout, M.P., Aitchison, J.D., 2001. The nuclear pore complex as a transport machine. J. Biol. Chem. 276, 16593–16596.
Sakiyama, Y., Panatala, R., Ryh, L., 2017. Structural dynamics of the nuclear pore complex. Semin. Cell Dev. Biol. 68, 27.
Solmaz, S., Chauhan, R., Blobel, G., Melčák, I., 2011. Molecular architecture of the transport channel of the nuclear pore complex. Cell 147, 590–602.
Stern, E., Wagner, R., Sigworth, F.J., Breaker, R., Fahmy, T.M., Reed, M.A., 2007. Importance of the Debye screening length on nanowire field effect transistor sensors. Nano Lett. 7, 3405.
Stoffler, D., Goldie, K.N., Feja, B., Aebi, U., 1999a. Calcium-mediated structural changes of native nuclear pore complexes monitored by time-lapse atomic force microscopy. J. Mol. Biol. 287, 741.
Stoffler, D., Goldie, K.N., Feja, B., Aebi, U., 1999b. Calcium-mediated structural changes of native nuclear pore complexes monitored by time-lapse atomic force microscopy 1. J. Mol. Biol. 287, 741–752.
Strambio-De-Castillia, C., Blobel, G., Rout, M.P., 1999. Proteins connecting the nuclear pore complex with the nuclear interior. J. Cell Biol. 144, 839–855.
Swift, J., Ivanovska, I.L., Buxboim, A., Harada, T., Dingal, P.C., Pinter, J., Pajerowski, J.D., Spinler, K.R., Shin, J.W., Tewari, M., 2013a. Nuclear lamin-A scales with tissue stiffness and enhances matrix-directed differentiation. Science 341, 975.
Swift, J., Ivanovska, I.L., Buxboim, A., Harada, T., Dingal, P.C.D.P., Pinter, J., Pajerowski, J.D., Spinler, K.R., Shin, J.W., Tewari, M., 2013b. Nuclear lamin-A scales with tissue stiffness and enhances matrix-directed differentiation. Science 341, 975.
Tschumperlin, D.J., Dai, G., Maly, I.V., Kikuchi, T., Laiho, L.H., Mcvittie, A.K., Haley, K.J., Lilly, C.M., So, P.T., Lauffenburger, D.A., 2004. Mechanotransduction through growth-factor shedding into the extracellular space. Nature 429, 83–86.
Wagner, O., Zinke, J., Dancker, P., Grill, W., Bereiter-Hahn, J., 1999. Viscoelastic properties of f-actin, microtubules, f-actin/ α -actinin, and f-actin/Hexokinase determined in microliter volumes with a novel nondestructive method. Biophys. J. 76, 2784–2796.
Wolf, C., Mofrad, M.R., 2008. On the octagonal structure of the nuclear pore complex: insights from coarse-grained models. Biophys. J. 95, 2073.
Yang, Q., Rout, M.P., Akey, C.W., 1998. Three-dimensional architecture of the isolated yeast nuclear pore complex: functional and evolutionary implications. Mol. Cell 1, 223.
Zhao, C.L., Mahboobi, S.H., Moussavibaygi, R., Mofrad, M.R., 2014. The interaction of CRM1 and the nuclear pore protein Tpr. Plos One 9, e93709.
Zhu, L., Wu, J., Liu, L., Liu, Y., Yan, Y., Cui, Q., Chen, X., 2016. Gating mechanism of mechanosensitive channel of large conductance: a coupled continuum mechanical-continuum solvation approach. Biomech. Model. Mechanobiol. 15, 1–20.